

# Supporting Information

Weijing Han et al. 10.1073/pnas.XXXXXXXXXX

## SI Text

**Human breast carcinoma tissue and second-harmonic generation (SHG) in collagen.** Carcinoma samples from two breast cancer patients were screened for this study. The tissue samples were embedded in paraffin, sectioned at a thickness of 3  $\mu\text{m}$  and stained with Hematoxylin-Eosin (HE).

Optical images of the tissue samples were acquired using an upright microscope (Ni-E, Nikon, Japan). The SHG of tissue samples were imaged by a two-photon microscope (A1R MP, Nikon, Japan) with a Mai Tai DeepSee laser, which generates 100-femtosecond pulse widths at a repetition rate of 80 MHz. The SHG signal of collagen was detected at wavelength range of 420–460 nm under 890-nm excitation light. In order to confirm that collagen fibers visualized in the SHG image are indeed abutting on tumor epithelium, the corresponding optical image of the HE-stained tissue were simultaneously viewed.

**3-D microdevice fabrication, surface modification and sandwiched gel formation.** Microdevice was fabricated by bonding a polydimethylsiloxane (PDMS) layer with desired microchannels to a cover glass. Microchannels were fabricated using soft-lithographic methods. The channels are composed of one ECM channel and two medium channels with micro patterned structures in 300  $\mu\text{m}$  depth as shown in Fig. 2 (A). In brief, PDMS was cast against a silicon master mold with microchannel features. After curing, PDMS replica was oxidized by oxygen plasma before it was bonded to the cover glass permanently. Prior to use, the microchannels were sterilized by immersing in 70% alcohol for 30 min. Then the channels were coated with 1 mg/mL poly-D-lysine (PDL) to prevent hydrogel detaching from channel walls after ECM filling.

Matrigel (100%, Corning, 356237) and 2.0 mg/mL collagen I (Corning, 354236) were used to form sandwiched gel. Fig. 2 (B1–B4) demonstrate detailed operation procedures of the sandwiched ECM structures construction with collagen I and Matrigel components. Fig. 2 (B1) is the enlarged picture displaying the centered pillar array structures in the PDMS chip. First, 15  $\mu\text{L}$  100% concentration of liquid Matrigel was loaded into the inlet of ECM channel with a pipette. Then the Matrigel flowed into the ECM channel with capillary force and filled the space. The gel edge had slightly periodical protrusions between the pillars with capillary force and obstruction of pillars, as is shown in Fig. 2 (B2). After that, 10  $\mu\text{L}$  liquid collagen I was loaded into inlet again. The pipette withdrew liquid gel at the outlet so that the negative pressure drove the collagen I through the Matrigel region along the mid-channel in laminar flow (Fig. 2 (B3)). After solidification, Matrigel and collagen I formed layered and wave-like boundaries. RPMI 1640 culture medium were injected into the shouldered channels afterwards (Fig. 2 (B4)).

## Sandwich-gel characterization.

**Interface of sandwiched ECM structure.** The interface between the two hydrogels of sandwiched ECM structure was characterized by observing FluoSpheres microspheres mixed into Matrigel

(yellow green,  $D=1\ \mu\text{m}$ , F-8823, Life Tech) and collagen I (dark red,  $D=0.2\ \mu\text{m}$ , F-8807, Life Tech). The sandwiched ECM structure with fluorescent microspheres was formed with previously mentioned method. The fluorescent images of the sandwiched ECM structure in z-axis were captured by a confocal laser-scanning microscope (Leica SP8, Germany) with a 10X objective lens and 25X water immersion lens. The captured images were reconstructed in 3-D using software LAS AF.

As shown in Fig. 2 (C1), the left panel is the bright-field picture of the Matrigel-collagen I morphology inside the channel. The collagen I and Matrigel was pre-mixed with red and green fluorescent beads respectively. The right panel indicates that the collagen I zone (red) replaced majority part of the Matrigel (green) in the middle and exhibited spindle-like shape inside. In order to further analyze the composite ECM structure in the vertical direction (z axis), the cross-sectional 3-D view along the marked green line in Fig. 2 (C1)) was characterized by the 3-D function of the confocal microscopy and shown in Fig. 2 (C2). It could be seen that the collagen I section is well packed by the Matrigel in the middle and present “tongue” like 3-D profiles.

**Sandwiched gel interface determination by cryo-Scanning Electron Microscopy (cryo-SEM).** To determine the interface of the sandwich-gel, cryo-SEM was performed which could minimize the dehydration of the gel matrix. The sandwiched gel was mounted on a slit holder and plunged into liquid nitrogen. Sample was then transferred to a PP3010T (Quorum) pre-chamber and cooled to  $-140\ ^\circ\text{C}$  under vacuum. A free-break surface was created with a cold knife, and the sample was sublimated at  $-85\ ^\circ\text{C}$  for 25 min, following by platinum sputter coating for 60 s. Then sample was transferred to the microscope cryo-stage at  $-130\ ^\circ\text{C}$  for imaging. The cryo-SEM images were captured by a field emission scanning electron microscope (FESEM, SU8010, Hitachi) using SE(L) detectors operating at 3 kV accelerating voltage, with magnifications varied from 1000X to 3000X.

Fig. 2 (C3) shows that the collagen I and Matrigel section had been linked well at the boundary but without any mixing or diffusion. Both of them had highly branched network and hollow structures, but Matrigel (right) presented a denser and more compact matrix than collagen I (left). The irregular micro-pores of Matrigel indicated its formation of continuous protein rather than fiber network as collagen I. And the linker proteins in Matrigel acted as a bridge to bound matrix proteins of the Matrigel and collagen I, which helped maintain the sharp interfaces of the sandwiched ECM. In overall, the collagen I region in the composite ECM was designed as the primary sector for tumor cell invasion. The Matrigel region, although thicker than the in vivo situation, was utilized to mimic basement membrane. This in vitro landscape would be a good simulation of tumor cell intravasation progression and help study the process and mechanism of the orientated collagen influence on cell invasion.

**Cell culture and staining.** The human breast carcinoma MDA-MB-231 (China Infrastructure of Cell Line Resource, Beijing, China) were cultured in RPMI 1640 (GIBICO, Life Tech) supplemented with 10% FBS, 100 U/mL penicillin, and 100 U/mL streptomycin at 37 °C with 5.0% CO<sub>2</sub>. Before loaded into the microchip, MDA-MB-231 cells were cultured in 7asks to 80% confluence and then detached using 0.25% trypsin-EDTA (Mediatech, Corning) solution. Collected cell suspension was centrifuged at 120 G for 5 min. Cells were re-suspended in RPMI medium. MDA-MB-231 cells were stained with CellMask<sup>TM</sup> Deep Red Plasma membrane Stain (Life Tech, U.S.A) for visualizing cell profiles. The nucleuses of cells were stained by Hoechst 33342 for tracking cell positions.

Cell suspension was mixed with collagen I on ice, with final density at 2.0 mg/mL, final pH value at 7.4 and cell density of 10<sup>6</sup>/mL. The collagen I with cells was then introduced into ECM channel that has been filled with liquid Matrigel, and then incubated at 37 °C for 30 min to form the sandwiched ECM. The medium channels were filled with culture medium with 25 ng/mL EGF after the sandwiched ECM solidification. As a comparison, only the collagen I with cells was directly injected into the ECM channel without Matrigel to analyze the differences of cells morphology in homogeneous collagen I and sandwiched ECM.

**Imaging of 3-D cell invasion in sandwiched ECM .** The 2-D and 3-D images of Hoechst stained cells in the sandwiched ECM were acquired by the confocal microscope. Each image scan took 6 min. Cells were put back into the incubator after each scanning. Time interval between two scans was constant 48 hours, which is an optimized condition to maximize the sampling rate without noticeable photodamage to the cells. The orientation of tumor cells in the sandwiched ECM was analyzed with the captured image sequences using ImageJ software. The tumor cells were tested in pure collagen I instead of sandwiched ECM as control experiments and the results were also analyzed with the same procedure.

#### Tumor cells' orientation analysis in homogeneous collagen.

A control experiment was performed to investigate the morphology of MDA-MB-231 cells in pure collagen I. 15  $\mu$ L cold liquid-state collagen was loaded into the microfluidic device from matrix inlet by a pipette. After injection, the collagen matrix was gelled in a humidified 5% CO<sub>2</sub> incubator at 37 °C for 30 min. Cell culture medium (RPMI1640+ 10% FBS+1% antibiotics+ 25 ng/mL EGF) was injected into the two medium channels after gelling of the ECM structure. The tumor cells (stained by Hoechst) observation was performed by the aforementioned confocal microscope.

**Cell invasion process from homogeneous collagen to Matrigel.** As shown in Supplementary Fig. S1(A), two holes (4 mm in diameter) were punched in a 3.5 mm thick PDMS layer as medium wells. A channel (2 mm wide) was formed in connection with the two holes.

In the experiment, 15  $\mu$ L liquid Matrigel was loaded into the Matrigel well and simultaneously, collagen I (2 mg/mL) mixed with MDA-MB-231 cells was loaded into the collagen well. After completely gelling, the medium well was filled with culture medium with 25 ng/mL EGF for long-term cell culture. The tumor cells (stained by Hoechst and CellMask<sup>TM</sup>) observation was performed by the confocal microscope. The

results proved that MDA-MB-231 cells were unable to invade the Matrigel at 100% concentration directly from homogenous collagen structures.

**Stress field in collagen I and Matrigel.** In order to understand the formation of fiber alignment in the collagen, the displacement field of beads in collagen and Matrigel were used to compute the stress field in the system. Since the goal here is only to qualitatively correlate local stress state to fiber reorientation, we assume that the mechanical displacement is proportional to the overall displacement. Moreover, linear elasticity is used which is a reasonable approximation of the mechanical behavior of the system.

The displacement field obtained via bead tracking is first interpolated on a regular cubic grid. In particular, natural neighbor interpolation is used, which is based on Voronoi tessellation of a discrete set of spatial points. The strain at the grid points (i.e., nodes) are then simply computed as the derivatives of the displacement field  $U$ , i.e.,

$$\epsilon = \partial U / \partial X. \quad [1]$$

To resolve the entire strain field, a proper shape function should be used to further interpolate the node strain to obtain the strain within an element of the system, similar to the standard procedure in a finite element analysis. Then stress can be easily calculated from the stress and strain relation based on linear elasticity. In the calculation, the following mechanical properties of the Matrigel and collagen are used: Young's modulus of Matrigel  $E_M = 450$  Pa, Poisson's ratio of Matrigel  $\nu_M = 0.49$ ; Young's modulus of collagen  $E_M = 100$  Pa, Poisson's ratio of collagen  $\nu_M = 0.33$ .

Fig. S2 shows the stress field in the collagen. It could be clearly seen that close to the collagen-Matrigel interface (i.e., the borders of collagen shown in the figure), the system is under tri-axial compression. This stress state could be understood as follows: as collagen extrudes into Matrigel, a flat interface is not stable and a convex extrusion front is developed. This extrusion is also responsible for the  $y$  component of the compressive normal stress. As the Matrigel swells, it "squeezes" the convex extrusion front of collagen, leading to large compressive normal stress  $\sigma_{xx}$  and  $\sigma_{zz}$ . Such a strong bi-axial stress state causes the reorientation of collagen fibers along the  $y$  direction in regions close to the extrusion front, which is consistent with the quantitative analysis of the confocal micrographs.

In the middle region of the collagen system that we analyzed, both the normal and shear stresses fluctuate, and thus could not lead to significant reorientation of the collagen fibers. This is consistent with the low degree of orientational correlations among the fibers observed in the confocal micrographs.

On the other hand, a large shear stress  $\tau_{yz}$  is observed in the bottom of the collagen system that was analyzed previously. As the collagen close to the extrusion front is squeezed to the middle, the collagen away from the front is also "dragged" to the middle, leading to the observed large shear stress  $\tau_{yz}$ . Such a shear stress, which could be considered as caused by the relative motion of two successive thin layers of collagen parallel to  $y$ - $z$  plane, could lead to significant fiber rotation and thus, realign along the  $x$ -direction. This is consistent with strong fiber alignment in that direction observed in the micrograph.

Finally, we note that in our analysis, elasticity is assumed for both Collagen I and Matrigel. It is well known that both materials may exhibit a certain level of viscoelastic behavior. We have varied the constitutive relations for the materials in the finite element analysis to incorporate the effects of viscoelasticity. The resulting stress field is qualitatively similar to the one obtained via elastic analysis.

**Computational model for 3-D single cell migration in ECM.** We propose a minimalist computational model that incorporates the 3-D cellular migration mechanisms and cell-ECM interactions for the mesenchymal mode. A change of protocol here will allow incorporating amoeboid migration mode. As illustrated in Fig. S3, our cell model consists of an elastic sphere representing the exclusion volume associated with cytoplasm and a set of actin filaments connecting the cytoplasm sphere to the plasma membrane. The plasma membrane is then modeled as the minimal hull associated with the end points of the filaments [see Fig. S3 (A)].

At the beginning of the simulation, a cell (i.e., a cytoplasm sphere and the associated actin filaments) is introduced in the collagen network. The collagen fibers close to the cell are represented by the sphere-chain model and remaining fibers are represented by the beam model. The migration process is decomposed into cycles of successive events including (i) development of protrusion, (ii) formation of new adhesion sites, (iii) degradation of collagen fibers, (iv) contraction of actin filaments (leading to the motion of the cell), and (v) breaking of old adhesion sites. These events are modeled and simulated as described below:

- Protrusions are generated by the elongation (polymerization) of the actin filaments that are not attached to the collagen fibers (referred as “free” actin filaments) (see Fig. S3 (B)). We consider each free filament could lead to a protrusion with probability  $p_s$ , which is proportional to the local concentration of adhesion sites  $\rho_a$  on the plasma membrane, i.e.,  $p_s \sim \rho_a$ . Thus, the development of protrusions is biased and more likely to occur in a region on the membrane with a large number of adhesion sites. The protrusion is approximated by a cone enclosing the elongated filament.
- If the surface of the protrusion is sufficiently close to a collagen fiber, a new adhesion site could form with a probability  $p_a$ ; see Fig. S3 (C). We consider the probability  $p_a$  is proportional to the local stress level  $\sigma_f$  (i.e.,  $\rho_a \sim \sigma_f$ ) of the fiber so that it is more likely to form an adhesion site on highly stressed fibers. Each adhesion site is considered to have a finite life span  $T_a$  and will break once its life span is reached.
- We consider that a migrating cell constantly degrades collagen fibers with a probability  $p_b \sim \exp(-r)$ , with  $r$  the distance from the fiber to the cell membrane. A degraded fiber is removed from the network in subsequent simulation steps.
- The contraction of an actin filament connected to a collagen fiber could generate a traction force  $f_t$  along the filament; see Fig. S3 (D). The total traction force  $F_t$  the cell feels is the sum of the forces generated by individual filaments, i.e.,  $F_t = \sum f_t$ . The cell also feels a resistance

force due to exclusion volume of the fibers. We consider the cell could change its shape when pushing through small pores and the exclusion volume effects are incorporated via the elastic interaction between the fibers and the cytoplasm sphere. The resulting total resistance force  $F_r$  is the sum of individual elastic repulsion forces proportional to volume of overlaps between the cytoplasm sphere and fibers. The displacement  $dr$  of cell is then computed by  $dr = \eta(F_r + F_t)dt$ , where  $\eta$  is an effective viscosity.

- All of the current adhesion sites are checked and those reaching their life span  $T_a$  are considered to break, leading to the detachment of the cell surface from the collagen fibers.

In the simulation, time is discretized such that an individual event occurs during the elapsing of one time step  $dt$ . During the contraction stage, the forces exerted on the collagen fibers will also be computed and the stress distribution in the collagen matrix and the deformation of the fibers are obtained by finite element calculations. Once an entire migration cycle is completed, the position of cytoplasm sphere is updated and the cell starts the next migration cycle. Our pilot studies suggested that  $dt \sim 1$  min could qualitatively reproduce the dynamics of experimentally observed 3-D mesenchymal cell migration.

**Single-cell Migration Simulations.** To illustrate the predictive capability of our model, we have employed it to simulate the migration of a single cell in model ECM networks with randomly oriented and aligned fibers. Fig. S4 shows the snapshots of the migration cells. Fig. S5 (A) shows the trajectory of a cell migrating in the “aligned” ECM network. The migration is clearly biased along the alignment direction, leading to an anisotropic trajectory. Fig. S5 (B) shows the trajectory of a cell migrating in the “random” ECM network. It could be seen that the motion of the cell has no preferred directions and the trajectory resembles that of a random walker, which is consistent with the previous studies using time-averaged dynamics model for cell migration. This is because the formation of the adhesion sites is biased by the aligned arrangement of the collagen fibers. Fig. S6 shows the velocity autocorrelation function  $f(t)$ , which is defined as follows:

$$f(t) = \int v(\tau) \cdot v(\tau + t) dt. \quad [2]$$

It could be clearly seen that the cell in the aligned network possesses a much longer persistence time than that in the random network, as manifested by the much slower decay of  $f(t)$  for the aligned ECM. These results indicate the validity and robustness of our cell migration model.

**Double-cell Migration Simulations.** To complement our experimental study and test the proposed mechanism for observed collective cell migration in heterogeneous ECM-matrigel system, we also investigate the migration dynamics of a pair of cells in model ECM networks. In particular, a homogeneous ECM structure and a heterogeneous network with aligned fibers, which mimic the actual experimental system. The ECM models are reconstructed based on 2-D confocal micrographs of different portions of ECM. The micrographs are

first coarse-grained to obtain an intensity map, whose standard two-point correlation functions are computed and fed into a stochastic reconstruction procedure to generate virtual 3-D intensity map with the same spatial statistics. Then the network structure, which is based on the “node-bond” (i.e., graph) representation, is reconstructed by distributing the nodes based on the 3-D intensity map and then optimizing the connectivity between the nodes such that distribution of coordination number, bond length as well as the nematic order metric of the reconstructed network match those computed from the 2-D micrographs up to a certain accuracy (e.g., the sum of squared difference between the simulated and experimental quantities is required to be small than  $10^{-3}$  in our simulations).

Snapshots of simulated migrating cell pairs in different ECM networks are shown in Fig. S7. It could be seen that in the heterogeneous network with a high degree of fiber alignment, the two migration cells exhibit stronger correlations. This could be also quantitatively seen in Fig. S8, which shows the normalized velocity correlation functions  $S(t)$  for cell pairs in different networks, which is defined as

$$S(t) = \int v_1(\tau + t) \cdot v_2(\tau + t) d\tau, \quad [3]$$

where  $v_1$  and  $v_2$  are the normalized velocity (i.e., with unitary norm) of the two cells. For the aligned fiber network, the directions of cell velocities are highly correlated, which are biased by the fiber alignment, leading to a  $S(t)$  with values slightly fluctuating close to unity. On the other hand, the velocities of the cells migrating in homogeneous ECM network with randomly orientated fibers are only weakly correlated, leading to a  $S(t)$  with large fluctuations around the mean value of zero, as shown in Fig. S8. In general, our numerical studies provide evidence for the hypothesis that cell invasion could be significantly enhanced via ECM mediated collective cell migration.

## SI Figures

SI Figure 1: Control experiment without fiber alignment was used to investigate the affection of aligned collagen on tumor cell invasion in *in vitro*.

SI Figure 2: The stress field in collagen.

SI Figure 3: Schematic illustration of the computational model for migrating cell.

SI Figure 4: Snapshots of simulated migrating cells.

SI Figure 5: Trajectory of simulated migrating cells.

SI Figure 6: Scaled velocity autocorrelation function.

SI Figure 7: Snapshots of simulated migrating cell pairs in different ECM networks.

SI Figure 8: Normalized velocity correlation functions.

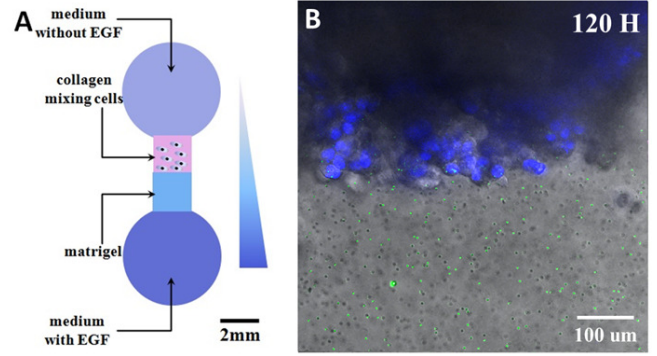
SI Figure 9: Characterization of the sandwiched gel swelling after immersion in medium.

SI Figure 10: Landscape plot of the collagen fiber orientation distribution in the sandwiched ECM.

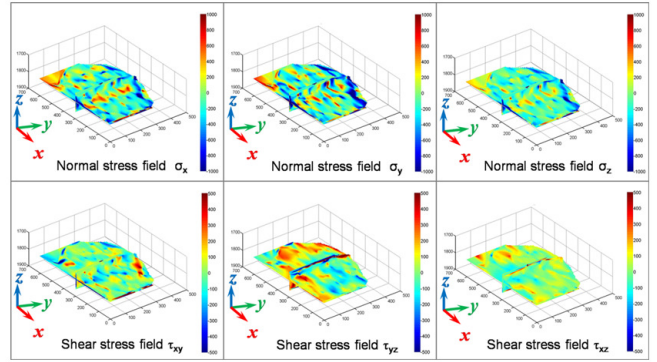
SI Figure 11: Characterization of the sandwiched ECM before immersion using reflection mode of the confocal microscope.

SI Figure 12: Characterization of the sandwiched ECM after immersion using reflection mode of the confocal microscope.

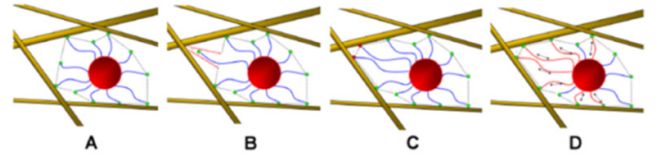
## SI Figure 13: Tumor cell orientation in homogeneous collagen.



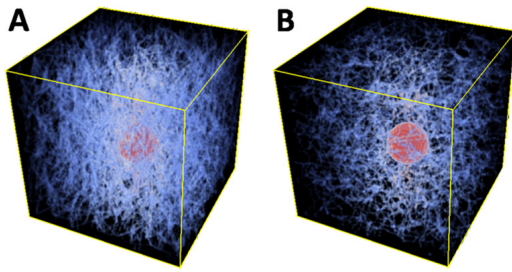
**Fig. S1.** Control experiment without fiber alignment was used to investigate the affection of aligned collagen on tumor cell invasion in *in vitro*. (A). Diagram sketch of the PDMS chip for this control experiment. The horizontal rectangular channel between the two chambers was filled with Matrigel (blue) and collagen homogeneously mixed with MDA-MB-231 (pink). The upper chamber was filled with medium without EGF, whereas the lower chamber was filled with medium with EGF (25 ng/mL). (B). MDA-MB-231 cells did not exhibit obviously invasion into Matrigel after 120 hours and was obviously different from the situation in the composite ECM.



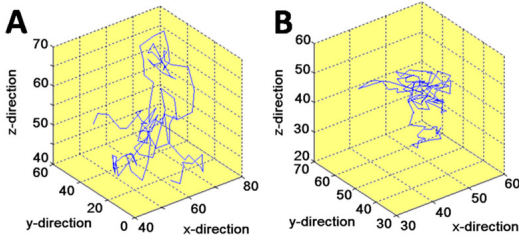
**Fig. S2.** The stress field in collagen: three orthogonal slices at (300, 200, 1800)  $\mu\text{m}$  are shown. The upper panels respectively shows the stress component  $\sigma_{xx}$ ,  $\sigma_{yy}$ ,  $\sigma_{zz}$  from left to right; and the lower panels shows the stress component  $\tau_{xy}$ ,  $\tau_{yz}$ ,  $\tau_{zx}$  from left to right. The unit of stress is Pa.



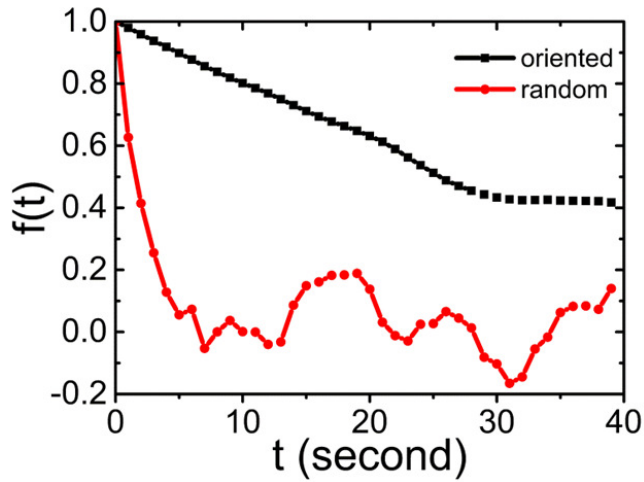
**Fig. S3.** Schematic illustration of the computational model for migrating cell. (A) The cell model that consists of an elastic sphere (red) representing the exclusion volume associated with cytoplasm and a set of actin filaments (blue) connecting the cytoplasm sphere to the plasma membrane (dashed line), modeled as the minimal hull associated with the end points of the filaments. (B) Development of protrusion by the elongation (polymerization) of free actin filaments. (C) Formation of new adhesion sites on the surface of protrusion. (D) Contraction of actin filaments which leads to the movement of the cell.



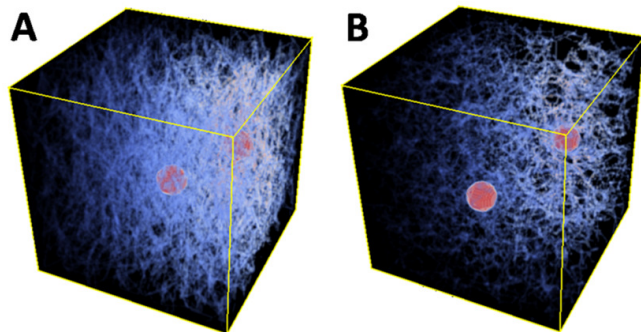
**Fig. S4.** Snapshots of simulated migrating cell in (A) oriented collagen network (B) random collagen network. The size of the simulation box shown is 60  $\mu\text{m}$ .



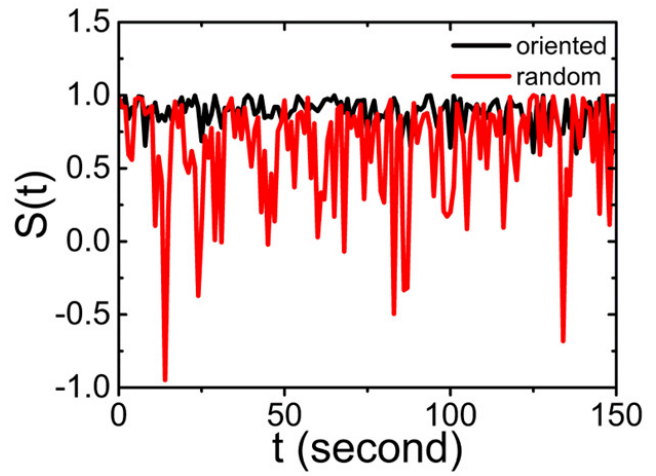
**Fig. S5.** Trajectory of simulated migrating cells in (A) oriented collagen network (B) random collagen network. The unit of distance is  $\mu\text{m}$ .



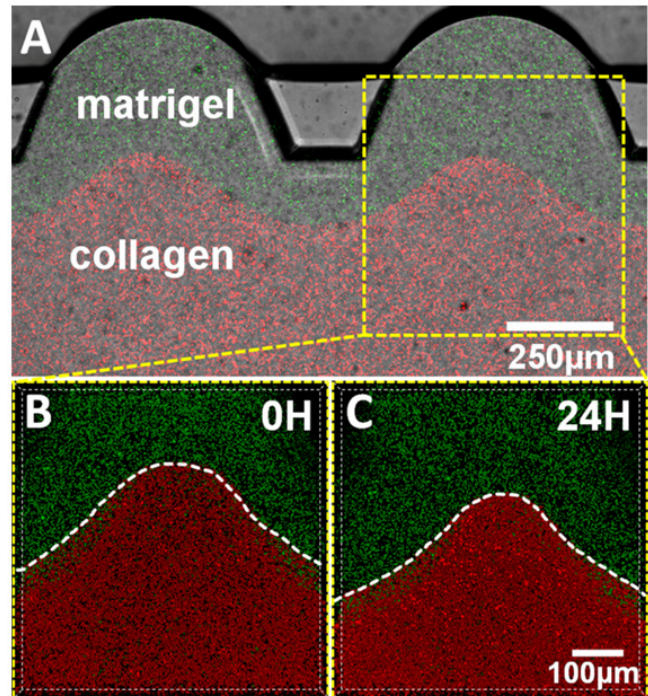
**Fig. S6.** Scaled velocity autocorrelation functions of simulated migrations cells in oriented and random collagen networks.



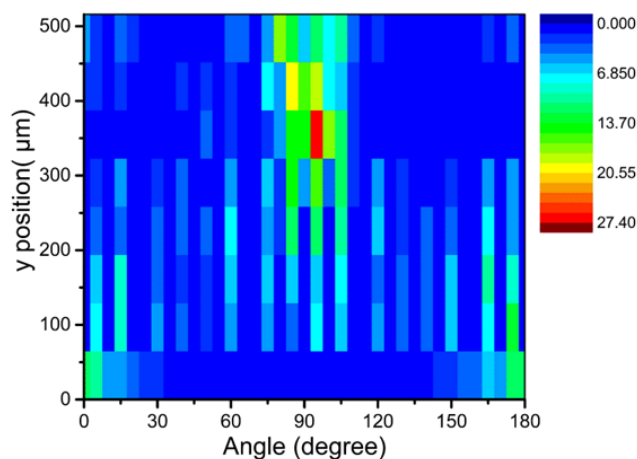
**Fig. S7.** Snapshots of simulated migrating cell pairs in different ECM networks. (A) Aligned network. (B) Random network.



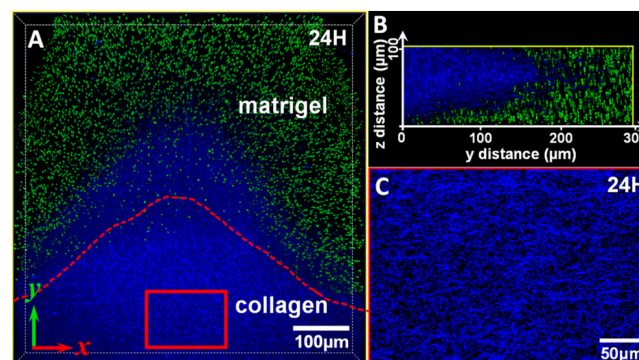
**Fig. S8.** Normalized velocity correlation functions  $S(t)$  for cell pairs in different networks.



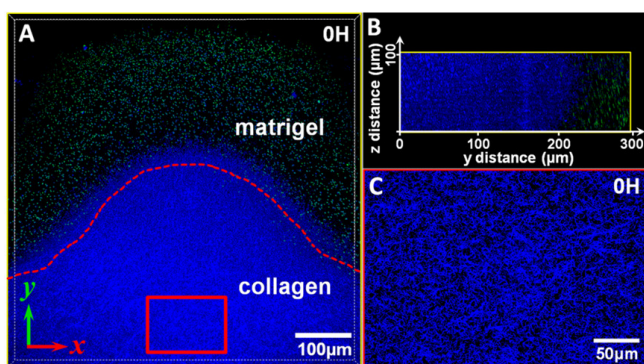
**Fig. S9.** Characterization of the sandwiched gel before and after immersion in medium. The plane view (A) of the sandwiched gel was obtained using confocal microscope. The z-stack images of the gelled sandwiched ECM before (B) and after immersion (C, after immersed into medium for 24 hours) were obtained using confocal microscope, and showed that interface between the collagen and Matrigel was reshaped during the immersion process but still clear.



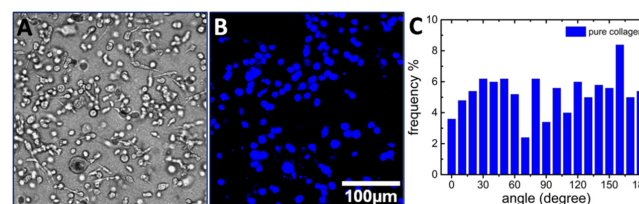
**Fig. S10.** Landscape plot of the distribution of collagen fiber orientation in the sandwiched ECM after immersion to culture medium. The distribution of collagen fiber orientation from the centered region gradually changed from 0 degree (or 180 degrees) to random orientation, and then 90 degrees. The landscape plot illustrated that the distribution of collagen fiber orientation was around 0 degree (parallel to the x direction near the middle part of the collagen region (0-65  $\mu\text{m}$  in y axis)). With the position change from the middle part of collagen region to the interface of the sandwiched ECM, the distribution of collagen fiber orientation gradually changed from 0 degree (or 180 degrees) to random orientation, and then 90 degree (65-325  $\mu\text{m}$  in y axis). There was more than 56% collagen fiber distributed between 85 degrees to 95 degrees at the interface of the sandwiched ECM (325-390  $\mu\text{m}$  in y axis). While in the Matrigel region (390-520  $\mu\text{m}$  in y axis), the concentration of collagen I was obviously decreased and the distribution of collagen fiber became disordered compared to the distribution at the interface.



**Fig. S12.** Characterization of the sandwiched ECM after immersion using reflection mode of the confocal microscope. After solidification, the sandwiched ECM was immersed in culture medium. Both of the z-axis 3-D confocal images and z-axis sectional view (A and B) showed that the interface of the sandwiched ECM was reorganized and presented that the protrusion tip region had horizontally orientated fiber structures. At the protrusion tip, majority of fibers became perpendicular to the Matrigel region. Besides, the majority of fibers in the collagen inner region displayed a distributed orientation to the ECM channel (C). The orientation might be induced by extrusion of osmotic pressure toward the center of the ECM channel, which was caused by ion or liquid exchange during immersion process as well as the volume swelling of Matrigel.



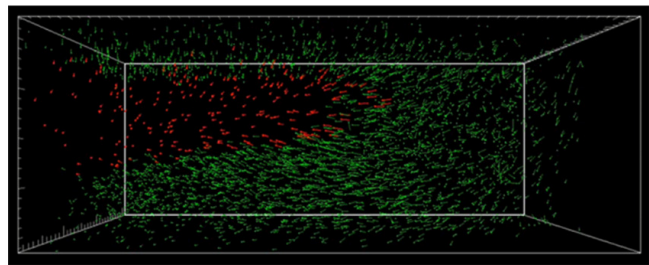
**Fig. S11.** Characterization of the sandwiched ECM before immersion using reflection mode of the confocal microscope. As shown in z-axis 3-D confocal images (A) and z-axis sectional view (B), the tip protrusion of the sandwiched ECM had a clear and uniform interface without obvious overlaps between green beads and the collagen region right after the sandwiched gel solidification. The red-box circled collagen fiber images in (A) was enlarged as shown in (C), which indicated that the collagen fibers near the middle part of the collagen zone was reshaped and formed random "bundles" after sandwiched gel injection and solidification, which was the result of the high viscosity of the Matrigel. The viscosity of Matrigel is ten times larger than that of collagen I (both of them are measured in liquid state). When collagen gel was injected into Matrigel, the shearing stress parallel with y direction might reshape the isotropic collagen into the horizontal state.



**Fig. S13.** Tumor cell orientation in homogeneous collagen. (A) and (B) are respectively the bright-field and fluorescent pictures of MDA-MB-231 cells in pure collagen. (C) is the statistical result of tumor cell orientation distribution in pure collagen. The results show that the cells exhibit individual proliferation with equal orientation distribution, which was in agreement with distribution of collagen fiber orientation in pure collagen.

**SI Movie**

**SI Movie:** Time-lapse movie of the sandwiched ECM during immersion process.



Time-lapse movie of the sandwiched ECM was used to analyze the mechanical process during immersion in detail (SI Movie). It shows that the entire immersion process was mainly divided into three steps: first, the sandwiched ECM extruded toward the center of the ECM channel (in the first frame) by osmotic pressure; then, the volume of Matrigel began increasing by ion or liquid exchange during immersion process (from second to seventh frame); finally, the volume change of Matrigel tended to be stabilized (from seventh frame to the last frame).